

# Direct growth of single- and few-layer MoS<sub>2</sub> on h-BN with preferred relative rotation angles

*Aiming Yan<sup>†, §, #</sup>, Jairo Velasco, Jr.<sup>†, #</sup>, Salman Kahn<sup>†</sup>, Kenji Watanabe<sup>⊥</sup>, Takashi Taniguchi<sup>⊥</sup>,  
Feng Wang<sup>†, §, #</sup>, Michael F. Crommie<sup>†, §, #</sup>, Alex Zettl<sup>†, §, #,\*</sup>*

<sup>†</sup>Department of Physics, University of California, Berkeley, CA 94720, USA

<sup>§</sup>Materials Sciences Division, Lawrence Berkeley National Laboratory, Berkeley, CA 94720,  
USA

<sup>⊥</sup>National Institute for Materials Science, 1-1 Namiki, Tsukuba, 305-0044, Japan

<sup>#</sup>Kavli Energy NanoSciences Institute at the University of California, Berkeley and the Lawrence  
Berkeley National Laboratory, Berkeley, CA 94720, USA

**KEY WORDS:** MoS<sub>2</sub>, CVD, heterostructure, h-BN, screw-dislocation driven growth

## **ABSTRACT:**

**Monolayer molybdenum disulphide (MoS<sub>2</sub>) is a promising two-dimensional direct-bandgap semiconductor with potential applications in atomically thin and flexible electronics. An attractive insulating substrate or mate for MoS<sub>2</sub> (and related materials such as graphene) is hexagonal boron nitride (h-BN). Stacked heterostructures of MoS<sub>2</sub> and h-BN have been produced by manual transfer methods, but a more efficient and scalable assembly method is needed. Here we demonstrate the direct growth of single- and few-layer MoS<sub>2</sub> on h-BN by a scalable chemical vapor deposition (CVD) method. The growth mechanisms for**

**single-layer and few layer samples are found to be distinct, and for single-layer samples low relative rotation angles (<5°) between the MoS<sub>2</sub> and h-BN lattices prevail. Moreover, MoS<sub>2</sub> directly grown on h-BN maintains its intrinsic 1.89 eV bandgap. Our CVD synthesis method presents an important advancement towards controllable and scalable MoS<sub>2</sub> based electronic devices.**

The realization of single-layer graphene on an insulating substrate<sup>1</sup> sparked renewed interest in van der Waals (vdW) bonded two-dimensional (2-D) materials including the exploration of new phenomena and potential applications. Transition metal dichalcogenides (TMDs) are well-known vdW 2D structures that can also be exfoliated in single atomic layer form onto insulating substrates. Notably, TMDs display many physical properties distinct from those of graphene. MoS<sub>2</sub> is a particularly noteworthy TMD in that it displays a direct electronic bandgap of 1.89 eV in single layer form and a smaller indirect gap for multi-layers. This transition allows much enhanced quantum yield of photoluminescence. Single-layer MoS<sub>2</sub> – based field effect transistors (FETs) exhibit high on/off ratio<sup>2</sup>, and control of valley polarization and coherence<sup>3</sup>. These properties establish MoS<sub>2</sub> as a promising candidate for flexible electronic, optoelectronic, and photonic applications.

Although for some applications suspended bare sheets of MoS<sub>2</sub> or other 2D materials is useful, in general the monolayers (or few layers) are mated to a substrate, either for mechanical stability or enhanced processibility, or to create a desirable electronic/optical heterostructure. The mate is often a 2D vdW material itself, and fabricating heterostructures comprised of different 2-D layered materials is a versatile approach that can integrate materials with different properties and realize new device functionalities<sup>4–6</sup>. Mating can be achieved through the manual transfer of individual 2-D layered materials or the direct growth of one type of 2-D material on

top of or adjacent to another<sup>7,8</sup>. Although the transfer method enables virtually any combination of layered materials in a heterostructure, it is tedious and effectively non-scalable. Direct transfer can also trap impurities or residues at the interface between individual layers during the transfer<sup>6,9</sup>. In contrast, direct growth of a 2-D layered material on top of or next to another is a more scalable and controllable method and yields clean interfaces<sup>7,8</sup>. Electrically insulating 2-D h-BN has been shown to be a superior substrate to SiO<sub>2</sub>/Si for graphene electronic devices due to the flat surface of h-BN and less charge inhomogeneity<sup>10-12</sup>. Similarly, it has also been shown that MoS<sub>2</sub> transferred onto h-BN exhibits excellent device quality<sup>13</sup>. The direct growth of MoS<sub>2</sub> on h-BN by CVD methods would be an important advance in fabricating high-quality MoS<sub>2</sub> electronic devices in a scalable and controllable way.

CVD growth of MoS<sub>2</sub> on different substrates has been investigated extensively in the past two years<sup>14,15</sup>, but growing MoS<sub>2</sub> directly on h-BN without any seeding method has not been previously reported. Here we demonstrate that single- and few-layer MoS<sub>2</sub> can be grown directly on exfoliated high-quality h-BN flakes using CVD. We find that the nominal growth mechanisms are different for single-layer and few-layer MoS<sub>2</sub>. Single-layer samples display low relative rotation angles (<5°) between the MoS<sub>2</sub> and h-BN lattices.

Figure 1(a) shows the two-zone furnace setup for CVD growth of single- and few-layer MoS<sub>2</sub> on exfoliated h-BN on SiO<sub>2</sub>/Si substrates. Unlike the reported one-zone furnace setup for the CVD growth of single-layer MoS<sub>2</sub> on bare SiO<sub>2</sub>/Si substrates<sup>14,15</sup>, a two-zone furnace allows the separate control of S and MoO<sub>3</sub> sources and enables greater tunability of the reaction process. The growth of single-layer MoS<sub>2</sub> on exfoliated h-BN is shown in the schematic in Fig. 1(b), where the green colored flake represents h-BN exfoliated on a SiO<sub>2</sub>/Si substrate and the isolated blue polygons represents single-layer MoS<sub>2</sub> flakes grown on the h-BN. Fig. 1(c) is an

optical image that depicts the typical end result of such a growth. The light green h-BN flakes are typically  $20 \times 10 \mu\text{m}^2$  and the dark green MoS<sub>2</sub> islands have typical size 2-3  $\mu\text{m}$  and are scattered randomly on the h-BN flake. On occasion, we also observe MoS<sub>2</sub> islands with higher optical contrast, suggesting growth of MoS<sub>2</sub> with layer number >1 is also possible (see below).

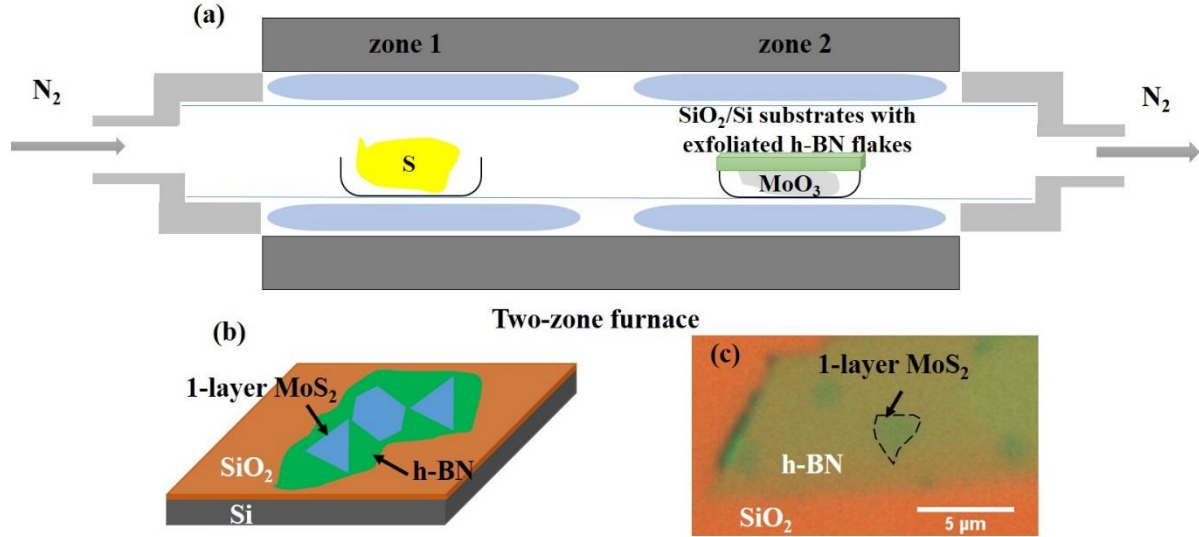


**Figure 1: Experimental setup for the growth, schematic and optical image for representative samples from the growth.** (a) Experimental setup for CVD growth of single- and few-layer MoS<sub>2</sub> on exfoliated h-BN. The quartz tube with S and MoO<sub>3</sub> precursors sits in the two-zone furnace. S is in zone 1 while MoO<sub>3</sub> precursor is in zone 2. Exfoliated h-BN flakes on SiO<sub>2</sub>/Si chips are placed on top of the crucible that has MoO<sub>3</sub> precursor. N<sub>2</sub> gas runs through the quartz tube during the whole growth process; (b) Schematic of the geometry of as-grown single- and few-layer MoS<sub>2</sub> on exfoliated h-BN flakes, which are on a SiO<sub>2</sub>/Si substrate. The green flakes represent thin h-BN (usually less than 200 nm thick) and blue flakes represent MoS<sub>2</sub> that have been grown on h-BN. (c) Optical image of a typical growth of MoS<sub>2</sub> islands on exfoliated thin h-BN flakes on SiO<sub>2</sub>/Si substrates. The lighter green flakes are h-BN and the darker green regions are typical MoS<sub>2</sub> flakes. An MoS<sub>2</sub> flake is outlined in (c).

We examine the atomic-level topography of the MoS<sub>2</sub> islands on h-BN via atomic force microscopy (AFM), as shown in Fig. 2. Three distinct MoS<sub>2</sub> island topographies are observed: (1) Flat and smooth MoS<sub>2</sub> islands (Figs. 2a (ii) and (iii)); (2) Flat and smooth MoS<sub>2</sub> islands that surround a tall protrusion at the center (Figs. 2b (ii) and (iii)); and (3) MoS<sub>2</sub> islands that exhibit striking helical fringes (Figs. 2c (ii) and (iii)).

We first focus on the (1) and (2) topographies because they are closely related; both represent single-layer MoS<sub>2</sub> growth and differ only in the size of the nucleation site. Both (1) and (2) topographies are usually isolated and located randomly on the h-BN flakes. A typical type (1) MoS<sub>2</sub> island is outlined with a blue box in Fig. 2a (ii); Fig. 2a (iii) shows a zoom-in of the boxed region. This MoS<sub>2</sub> island is  $\sim 4 \mu\text{m}^2$  in area, which is common for type (1) growth. Often, the MoS<sub>2</sub> islands of type (1) are polygon-shaped. A line profile from the edge of the MoS<sub>2</sub> island in Fig. 2a (iii) is shown in Fig. 2a (iv). The step edge profile reveals a height of  $\sim 0.7\text{nm}$ , consistent with the height of a single layer of MoS<sub>2</sub><sup>2,16</sup>. Although not revealed in Fig. 2(a), the likely nucleation site for the MoS<sub>2</sub> island in type (1) growth is a small defect in the h-BN, for example a point vacancy<sup>17</sup>.

In Fig. 2b (ii), a flat and smooth MoS<sub>2</sub> island of topography (2), which surrounds a tall protrusion at the center, is outlined with a blue box. Fig. 2b (iii) shows a zoom-in of the boxed region. MoS<sub>2</sub> islands of type (2) are typically flat and smooth with area  $1 \mu\text{m}^2 - 4 \mu\text{m}^2$ , and often have a flower-petal like shape. The tall protrusion in the center is usually smaller than 500 nm and has a polygon-like shape. Fig. 2b (iv) and its inset shows an AFM line scan, consistent with single-layer MoS<sub>2</sub>. The tall pillar-like protrusion in the center of the MoS<sub>2</sub> monolayer island is  $\sim 25\text{ nm}$  tall and is itself composed of multi-layer MoS<sub>2</sub>. The pillar likely marks a rather drastic nucleation site in the underlying h-BN, such as a triangular multi-atom defect<sup>17,18</sup> or impurities

on the surface of h-BN. With increased growth time, such a pillar will nucleate multi-layer MoS<sub>2</sub> (typically 10 layers or less) over an extended region, much like the extended lower branches of a Christmas tree. The growth of the single-layer islands of type (1) and (2) is depicted schematically in Figs. 2a (i) and 2b (i).

Fig. 2c (ii) shows an example of topography (3), which is distinct from topographies (1) and (2): the MoS<sub>2</sub> islands are pyramid-like with hexagonal or triangular bases. The type (3) islands are of different maximum thickness and are located randomly on the h-BN flakes. Interestingly, the type (3) islands have a helical (spiral) structure in the normal direction. Fig. 2c (iii) shows a zoom-in image of one of the islands, and Fig. 2c (iv) shows the result of an AFM line scan acquired along the red line of Fig. 2c (iii)). The entire island structure identified here has a height of ~10 nm and step-like features with 0.86 nm heights. This clearly represents multi-layer MoS<sub>2</sub>, grown in a screw-like manner.

Topography (3) multilayer MoS<sub>2</sub> islands result from a screw-dislocation-driven (SDD) growth mechanism. This has also been observed in other CVD grown TMD materials <sup>19,20</sup> and has been attributed to a low supersaturation condition. The SDD growth mechanism is also a common growth mode observed in other anisotropic nanostructure growths<sup>21-23</sup>. We depict this growth in Figure 2c (i) as a cross-sectional schematic of multilayer MoS<sub>2</sub> grown on h-BN. For SDD growth of a 2-D material, the starting point is typically a vertical offset (or slip) in the atomic planes of the first growth layer. Both the helical features and the profile with a step height of 0.86 nm, which is close to the thickness of single-layer MoS<sub>2</sub>, indicates the type (3) multi-layer islands of MoS<sub>2</sub> represent SDD growth with a single elementary Burgers vector for the screw dislocation<sup>19,24</sup>. We have also observed herringbone contours (Fig. s1) in few-layer MoS<sub>2</sub> grown on h-BN, which are typical features in SDD growth<sup>19,24</sup>.

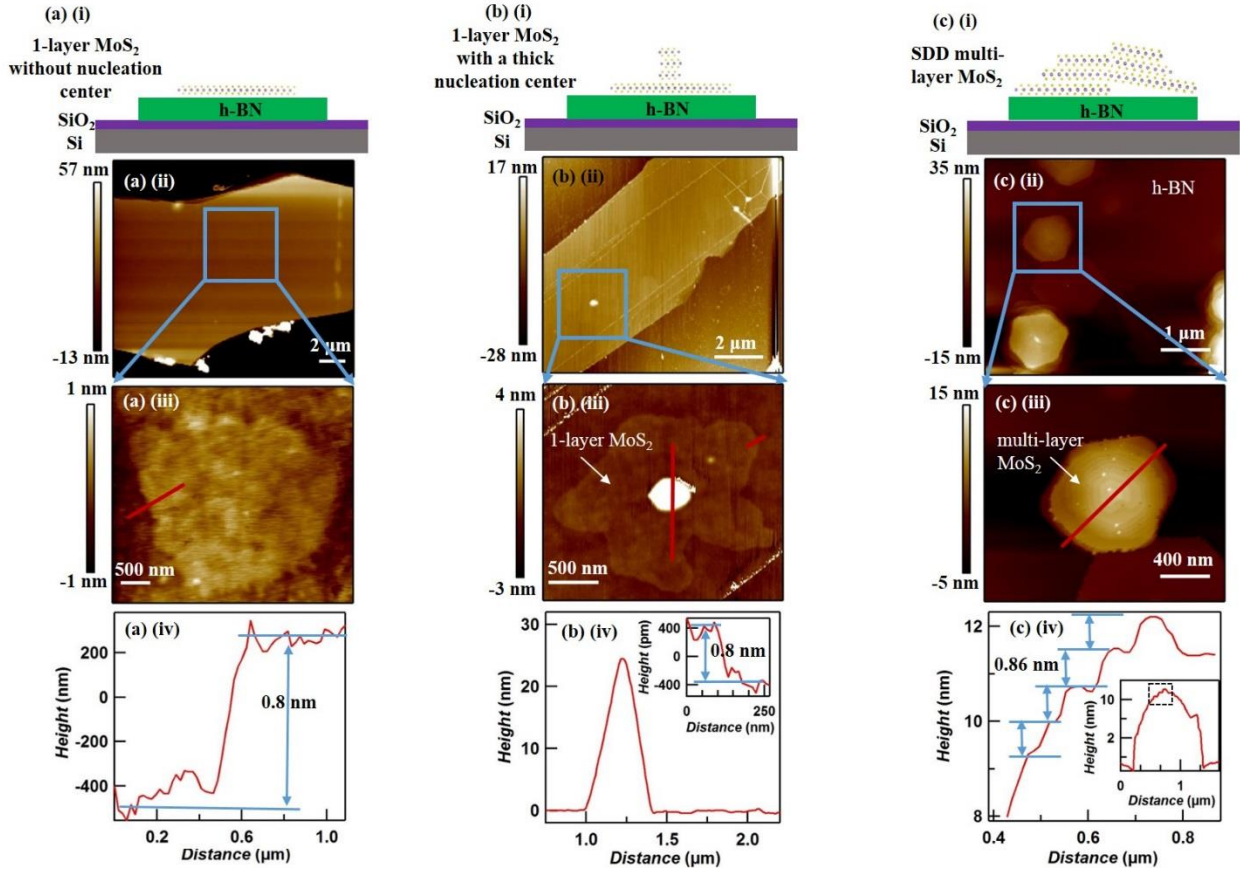


**Figure 2: AFM characterization of single-layer and multi-layer MoS<sub>2</sub> grown on exfoliated h-BN, which shows different growth mechanisms of MoS<sub>2</sub> on exfoliated h-BN by CVD method.**

(a)(b) both show the typical geometry of single-layer MoS<sub>2</sub> grown on h-BN. (a) shows a single-layer MoS<sub>2</sub> without a nucleation center can grow on h-BN. (a) (i) is the schematic of such growth. The green slab represents an h-BN flake and the sandwich-structured MoS<sub>2</sub> is grown on top. (a) (ii) is the low-magnification AFM image of single-layer MoS<sub>2</sub> on h-BN and (a) (iii) is the zoom-in image of the area outlined by the blue box in a(ii). The height profile at the edge of MoS<sub>2</sub> shows the thickness is around 0.7 nm, which is consistent with single-layer MoS<sub>2</sub>. (b) (i) shows the schematic for single-layer MoS<sub>2</sub> with a thick nucleation center. (b) (ii) shows the low-magnification AFM image of a single-layer MoS<sub>2</sub> with a thick nucleation center on h-BN and b(iii) is the zoom-in image of the MoS<sub>2</sub> flake outlined in b(ii). b(iii) is the height profile across

*the nucleation center and the edge of MoS<sub>2</sub>, showing the nucleation center is around 25 nm, while the edge shows a thickness of a single-layer MoS<sub>2</sub>. c(i) is the schematic for multi-layer MoS<sub>2</sub> grown on h-BN. A typical multi-layer MoS<sub>2</sub> island grown on h-BN follows the screw-dislocation-driven (SDD) growth mechanism. c(i) shows the growth starts from a screw-dislocation created at the interface of two MoS<sub>2</sub> flakes with one elementary burgers vector displaced vertically. c(ii) is the low-magnification AFM image of a few multi-layer MoS<sub>2</sub> islands grown on h-BN. c(iii) shows the zoom-in image of one MoS<sub>2</sub> island outlined in c(ii). The height profile across the center of MoS<sub>2</sub> island in c(iv) shows the step size of ~0.86 nm, which is about the thickness of one-layer MoS<sub>2</sub>. The color scale for all the AFM images is adjusted so that as-grown MoS<sub>2</sub> flakes can be visualized from the contrast.*

We employ transmission electron microscopy (TEM) to further characterize MoS<sub>2</sub> grown on h-BN. Fig. 3a shows for a type (2) multi-layer MoS<sub>2</sub> island the high-angle-annular-dark-field (HAADF) image. Since MoS<sub>2</sub> is atomically heavier than h-BN the HAADF image will show significant contrast between MoS<sub>2</sub> and h-BN. Indeed, in Fig. 3a we observe a bright triangular area on top of a distinct dark background, representing the presence of MoS<sub>2</sub> on h-BN. Energy-dispersive X-ray spectroscopy (EDS) mapping with distributions of Mo, S, B and N are also shown in Fig. 3(b-e), respectively. In this EDS mapping, B and N are found in the entire area indicating h-BN is present everywhere within the observation window, as expected. Mo and S are distributed in a manner similar to the shape of the bright contrast in Fig. 3a, and are clearly attributed to MoS<sub>2</sub>. EDS analysis also allows the Mo:S ratio to be determined; we find 36.6 to 63.4, consistent (considering experimental uncertainties) with the expected composition 1:2 for MoS<sub>2</sub>. Our TEM EDS measurements thus unambiguously confirm the flakes grown in this study as MoS<sub>2</sub>.

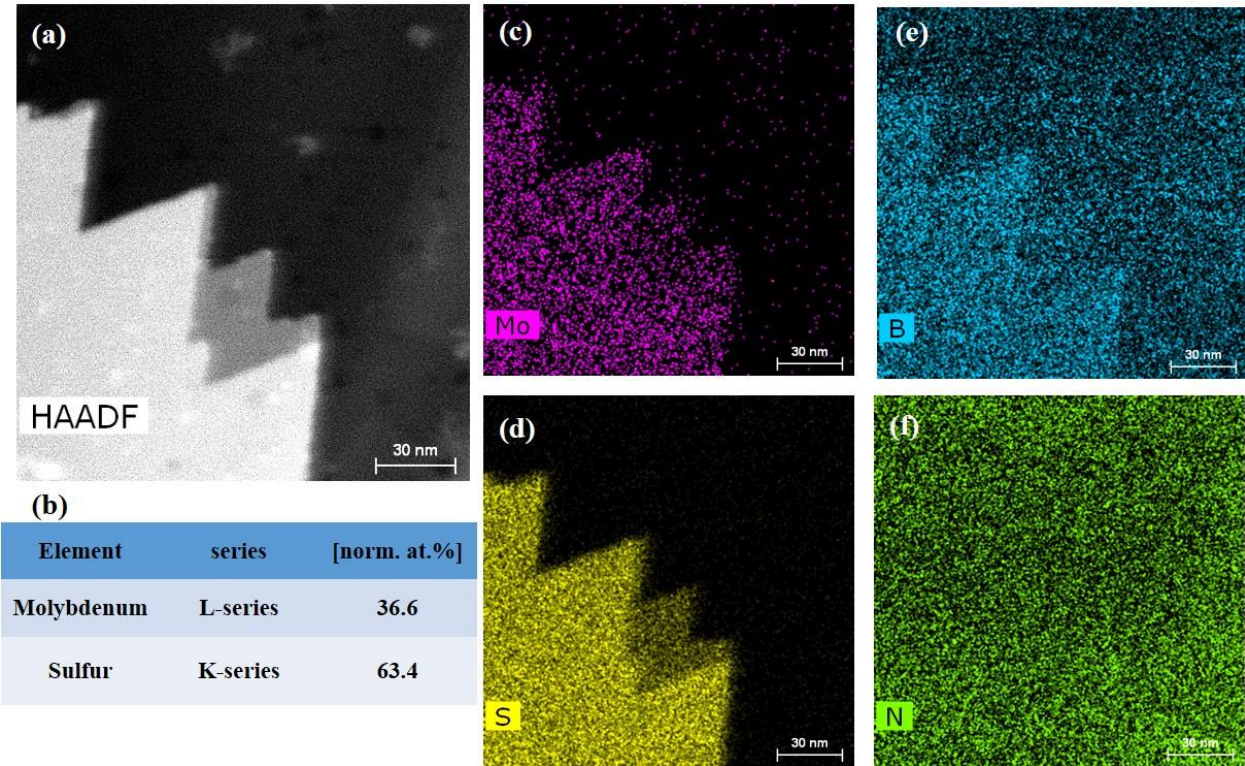


**Figure 3: STEM EDS mapping of thin MoS<sub>2</sub> grown on exfoliated h-BN, showing the composition/stoichiometry of MoS<sub>2</sub> flakes on h-BN.** (a) High-angle-annular-dark-field (HAADF) image of few-layer MoS<sub>2</sub> on h-BN. The white region is as-grown thin MoS<sub>2</sub> while the dark background is h-BN. (c)(d)(e)(f) are the elemental maps of MoS<sub>2</sub> on h-BN, showing the location of Mo, S, B and N respectively. The Mo and S maps clearly show the MoS<sub>2</sub> flake. N map shows uniform distribution while B map shows higher intensity around the location of the MoS<sub>2</sub> flake. The non-uniform distribution of B is due to the overlap of the B and Mo peaks in the spectrum (figure s2): the concentration of B is based on the intensity of the B peak around 0.18 keV and this B peak may include some intensity from the Mo peak located around the same energy. (b) provides the atomic composition of Mo (36.6%) and S (63.4%), analyzed from the STEM EDS mapping. The atomic ratio between Mo and S is close to the expected 1:2 for MoS<sub>2</sub>.

To characterize the quality of monolayer MoS<sub>2</sub> crystals grown on h-BN, we perform photoluminescence (PL) experiments (Fig. 4), and compare the results to PL measurements on single-layer MoS<sub>2</sub> grown on SiO<sub>2</sub> via CVD. AFM is used to ensure that the MoS<sub>2</sub> samples are single layer. Our single-layer MoS<sub>2</sub> grown on h-BN has a strong PL peak centered at 1.89 eV (Fig. 4). This measured direct band gap is quite close to the one of free-standing exfoliated single-layer MoS<sub>2</sub>- 1.90 eV<sup>25</sup>, and is larger than the CVD grown MoS<sub>2</sub> on SiO<sub>2</sub> (1.84eV<sup>14</sup>) and exfoliated single-layer MoS<sub>2</sub> on SiO<sub>2</sub> (1.85eV<sup>26</sup>). The full width at half maximum (FWHM) of the PL peak from as-grown MoS<sub>2</sub>/h-BN heterostructure is approximately 40 meV, which is slightly smaller than that for CVD grown MoS<sub>2</sub> on SiO<sub>2</sub> (50 meV) as shown in Fig. 4 and also in reference<sup>14</sup>) and free-standing exfoliated MoS<sub>2</sub> (50-60 meV<sup>25</sup>), and is much smaller than MoS<sub>2</sub> exfoliated onto SiO<sub>2</sub> (100- 150 meV<sup>26</sup>). These characteristics of PL indicate that MoS<sub>2</sub> grown on h-BN is electronically less perturbed than that grown on SiO<sub>2</sub>, and is more like free-standing MoS<sub>2</sub>.

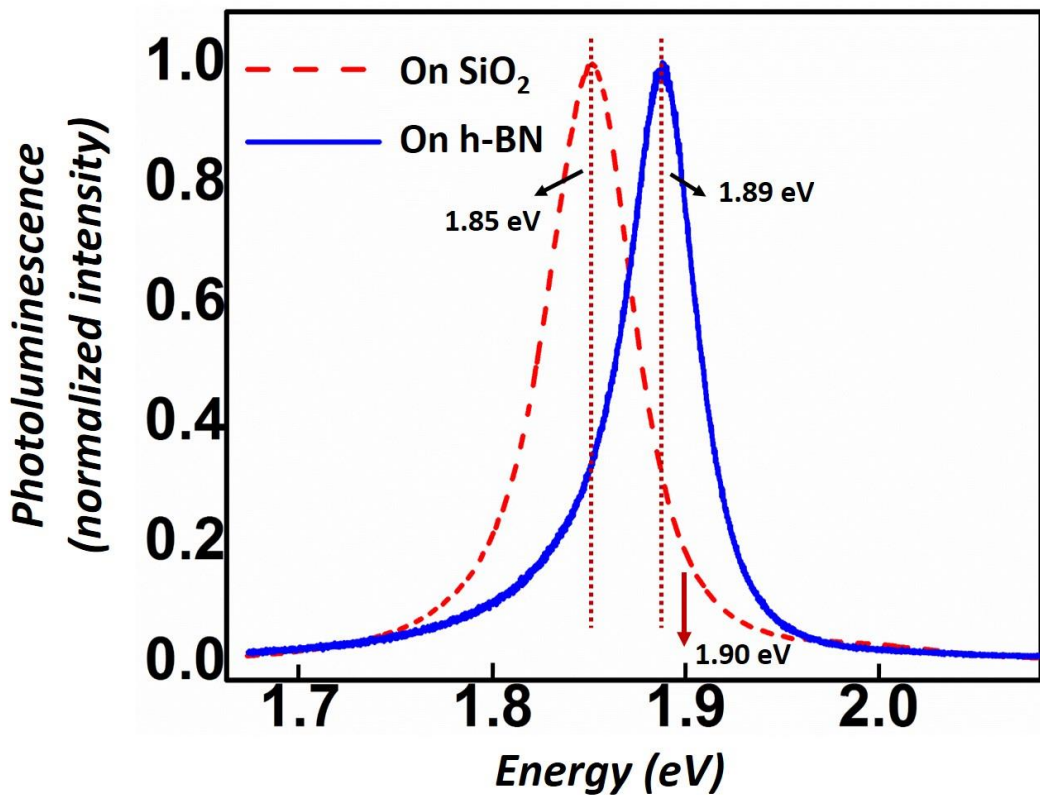


**Figure 4: Photoluminescence from single-layer MoS<sub>2</sub> grown on h-BN.** Photoluminescence peak from single-layer MoS<sub>2</sub> grown on h-BN (1.89 eV) indicates a band gap closer to free-standing MoS<sub>2</sub> flake (1.90 eV, pointed out by the arrow) compared to that grown on SiO<sub>2</sub> (1.85 eV).

We now turn to the relative crystal orientation of MoS<sub>2</sub> grown on h-BN. The relative rotation angle between the constituent layers in a 2-D heterostructure can play a significant role in the electronic band structure of the heterostructure<sup>7,27,28</sup>. Here we use selected area electron diffraction (SAED) in TEM to study the relative rotation angle between single/multi-layer MoS<sub>2</sub> and the h-BN substrate. In general, we find that the relative rotation angle for both single-layer and multi-layer MoS<sub>2</sub> grown on h-BN is not unique. Nevertheless, our statistical study of single-layer MoS<sub>2</sub> grown on h-BN indicates there is preference for particular angles.

We focus on single-layer MoS<sub>2</sub>/h-BN heterostructure and characterize the rotation angle for ~20 of our grown flakes. Fig. 5a shows a typical SAED pattern taken from a region that includes single-layer MoS<sub>2</sub> and h-BN. In this pattern, there are two sets of six-fold symmetric diffraction spots. The six spots of the inner hexagon (denoted by green lines) corresponds to MoS<sub>2</sub> ( $a_{\text{MoS}_2} = 3.1 \text{ \AA}$ ) and the six spots of the outer hexagon (denoted by purple lines) corresponds to h-BN ( $a_{\text{h-BN}} = 2.5 \text{ \AA}$ ). From this diffraction pattern we measure a relative rotation angle between MoS<sub>2</sub> and h-BN of ~9°. By selecting one diffraction spot of MoS<sub>2</sub>, one can visualize the MoS<sub>2</sub> flake in dark field image (Figure 5b), where MoS<sub>2</sub> appears bright and the dark background is h-BN. Based on the area probability histogram for specific relative rotation angles between the as-grown single-layer MoS<sub>2</sub> and h-BN (from ~20 locations), a low angle (< 6°) is most dominant (around 45% area fraction), as shown in Fig. 5(c). Single-layer MoS<sub>2</sub> flakes that have a relative rotation angle 6°-12° and 24°-30° are also present but are less prevalent. This variation can be attributed to the large lattice mismatch between MoS<sub>2</sub> and h-BN, which allows different structural relaxations of MoS<sub>2</sub> on h-BN during the high-temperature growth.

The study of relative rotation angle between multi-layer MoS<sub>2</sub> and h-BN substrate is more complicated due to the more complex growth mechanism of multi-layer MoS<sub>2</sub> islands grown on h-BN compared to the single-layer MoS<sub>2</sub> case. In this case we often observe multiple relative rotation angles although the h-BN substrate may be one single-crystal domain. Fig. 5(d) shows a triangular MoS<sub>2</sub> thick island grown on h-BN. The significant contrast at the center of the MoS<sub>2</sub> flake is caused by the screw-dislocation. The SAED pattern taken from the outlined area in Fig. 5(d) is shown in Fig. 5(e). There are at least two relative rotation angles in Fig. 5(e), but one strongly apparent and symmetric set of diffraction spots from MoS<sub>2</sub> shows the relative rotation

angle is  $3^\circ$ , which is consistent with the most probable relative rotation angle for single-layer MoS<sub>2</sub> grown on h-BN as shown in Fig. 5(c).

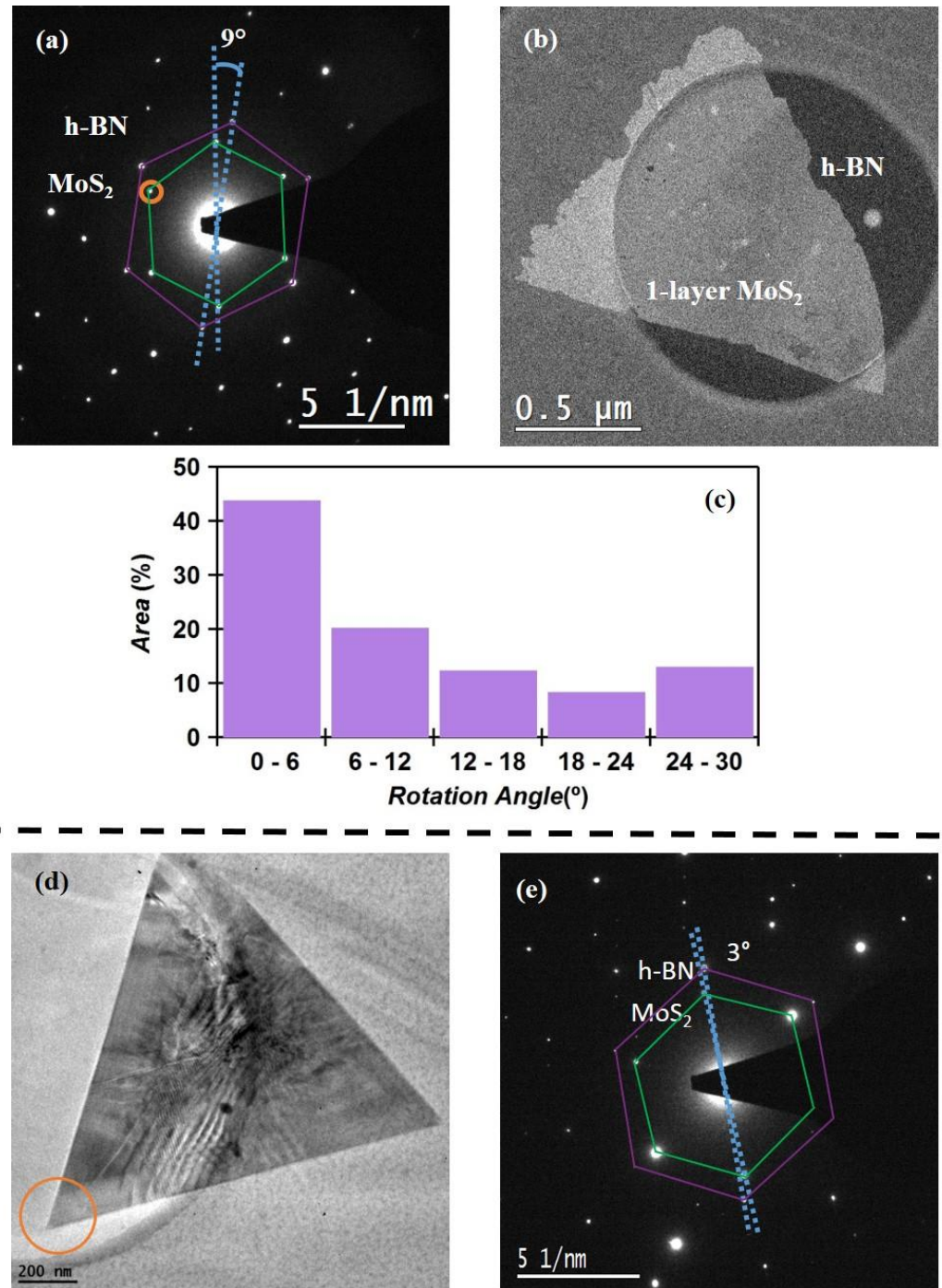


**Figure 5: TEM characterization of single-layer and multi-layer MoS<sub>2</sub> grown on exfoliated h-BN.** (a) A typical selected area electron diffraction (SAED) pattern of a single-layer MoS<sub>2</sub> flake grown on thin h-BN. The green hexagon shows the six-fold-symmetric diffraction spots from MoS<sub>2</sub> while the purple hexagon shows the six-fold-symmetric diffraction spots from h-BN. The relative rotation angle between MoS<sub>2</sub> and h-BN is measured to be 9° from this diffraction pattern. By selecting one of the diffraction spots from MoS<sub>2</sub> (outlined in (a)), one can visualize the MoS<sub>2</sub> flake in dark field image shown in (b). The white region in (b) is the single-layer MoS<sub>2</sub> while h-BN appears dark. The white dot visible on h-BN is residual polymer from TEM sample preparation, which also indicates the dark region is not empty. The heterostructure of MoS<sub>2</sub> and h-BN lies over a hole on a quantifoil TEM grid. (c) shows the area probability histogram of the relative rotation angle of single-layer MoS<sub>2</sub> grown on h-BN based on ~ 20 locations of such growth. (d) is a TEM image of a typical triangular multi-layer MoS<sub>2</sub> island grown on h-BN. The contrast due to the screw dislocation is visible around the center of MoS<sub>2</sub> island. (e) is the diffraction pattern from the region outlined in (d). The green hexagon outlines the diffraction spots from MoS<sub>2</sub> while the purple hexagon outlines the diffraction spots from h-BN. The relative rotation angle between MoS<sub>2</sub> and h-BN at this specific location is ~3°.

In summary, we have demonstrated that single-layer and few-layer MoS<sub>2</sub> can be directly grown on h-BN by CVD method. The growth mechanisms were found to differ depending on the different supersaturation condition of precursors. Under low supersaturation condition, screw-dislocation-driven growth dominates and causes the few-layer MoS<sub>2</sub> to form striking helical structures. Otherwise, single-layer and few-layer MoS<sub>2</sub> with non-observable or observable nucleation centers can form on h-BN. The as-grown single-layer MoS<sub>2</sub> on h-BN shows a strong photoluminescence peak centered around 1.89 eV, which is closer to that of free-standing MoS<sub>2</sub>.

This indicates single-layer MoS<sub>2</sub> grown on h-BN has less perturbed electrically environment and is promising for high-quality MoS<sub>2</sub>-based devices. Detailed TEM studies show that single-layer MoS<sub>2</sub> grown on h-BN has preferred low relative rotation angle between the two, which is also interesting for further study of electronic band structure modification due to different relative rotation angle in this heterostructure.

## ASSOCIATED CONTENT

**Supporting Information:** Including “Materials and methods”, Figure S1 and S2. This material is available free of charge via the internet at <http://pubs.acs.org>.

## AUTHOR INFORMATION

### Corresponding Author

\*To whom correspondence should be addressed: azettl@berkeley.edu

## ACKNOWLEDGEMENT:

This research was supported in part by the Director, Office of Basic Energy Sciences, Materials Sciences and Engineering Division, of the U.S. Department of Energy under Contract DE-AC02-05CH11231, within the sp<sub>2</sub>-bonded Materials Program, which provided for postdoctoral support and AFM and PL characterization by NSF grant DMR-1206512 which provided for the sample growth; and by the Molecular Foundry of the Lawrence Berkeley National Laboratory, under Contract DE-AC02-05CH11231, which provided for TEM characterization.

## REFERENCE:

- (1) Novoselov, K. S.; Geim, A. K.; Morozov, S. V; Jiang, D.; Zhang, Y.; Dubonos, S. V; Grigorieva, I. V; Firsov, A. A. Electric Field Effect in Atomically Thin Carbon Films. *Science* (80-). **2004**, *306*, 666–669.
- (2) Radisavljevic, B.; Radenovic, A.; Brivio, J.; Giacometti, V.; Kis, A. Single-Layer MoS<sub>2</sub> Transistors. *Nat. Nanotechnol.* **2011**, *6*, 147–150.
- (3) Xu, X.; Yao, W.; Xiao, D.; Heinz, T. F. Spin and Pseudospins in Layered Transition Metal Dichalcogenides. *Nat. Phys.* **2014**, *10*, 343–350.
- (4) Wang, L.; Meric, I.; Huang, P. Y.; Gao, Q.; Gao, Y.; Tran, H.; Taniguchi, T.; Watanabe, K.; Campos, L. M.; Muller, D. A.; *et al.* One-Dimensional Electrical Contact to a Two-Dimensional Material. *Science* (80-). **2013**, *342*, 614–617.
- (5) Mayorov, A. S.; Gorbachev, R. V; Morozov, S. V; Britnell, L.; Jalil, R.; Ponomarenko, L. A.; Blake, P.; Novoselov, K. S.; Watanabe, K.; Taniguchi, T.; *et al.* Micrometer-Scale Ballistic Transport in Encapsulated Graphene at Room Temperature. *Nano Lett.* **2011**, *11*, 2396–2399.
- (6) Kretinin, A. V; Cao, Y.; Tu, J.-S.; Yu, G.; Jalil, R.; Novoselov, K. S.; Haigh, S.; Gholinia, A.; Mishchenko, A.; Lozada, M.; *et al.* Electronic Properties of Graphene Encapsulated with Different 2D Atomic Crystals. *Nano Lett.* **2014**.
- (7) Yang, W.; Chen, G.; Shi, Z.; Liu, C.-C.; Zhang, L.; Xie, G.; Cheng, M.; Wang, D.; Yang, R.; Shi, D.; *et al.* Epitaxial Growth of Single-Domain Graphene on Hexagonal Boron Nitride. *Nat. Mater.* **2013**, *12*, 792–797.
- (8) Gong, Y.; Lin, J.; Wang, X.; Shi, G.; Lei, S.; Lin, Z.; Zou, X.; Ye, G.; Vajtai, R.; Yakobson, B. I.; *et al.* Vertical and in-Plane Heterostructures from WS<sub>2</sub>/MoS<sub>2</sub> Monolayers. *Nat. Mater.* **2014**.
- (9) Haigh, S. J.; Gholinia, A.; Jalil, R.; Romani, S.; Britnell, L.; Elias, D. C.; Novoselov, K. S.; Ponomarenko, L. A.; Geim, A. K.; Gorbachev, R. Cross-Sectional Imaging of Individual Layers and Buried Interfaces of Graphene-Based Heterostructures and Superlattices. *Nat. Mater.* **2012**, *11*, 764–767.
- (10) Dean, C. R.; Young, A. F.; Meric, I.; Lee, C.; Wang, L.; Sorgenfrei, S.; Watanabe, K.; Taniguchi, T.; Kim, P.; Shepard, K. L.; *et al.* Boron Nitride Substrates for High-Quality Graphene Electronics. *Nat. Nanotechnol.* **2010**, *5*, 722–726.
- (11) Xue, J.; Sanchez-Yamagishi, J.; Bulmash, D.; Jacquod, P.; Deshpande, A.; Watanabe, K.; Taniguchi, T.; Jarillo-Herrero, P.; LeRoy, B. J. Scanning Tunnelling Microscopy and Spectroscopy of Ultra-Flat Graphene on Hexagonal Boron Nitride. *Nat. Mater.* **2011**, *10*, 282–285.

(12) Decker, R.; Wang, Y.; Brar, V. W.; Regan, W.; Tsai, H.-Z.; Wu, Q.; Gannett, W.; Zettl, A.; Crommie, M. F. Local Electronic Properties of Graphene on a BN Substrate via Scanning Tunneling Microscopy. *Nano Lett.* **2011**, *11*, 2291–2295.

(13) Lee, G.-H.; Yu, Y.-J.; Cui, X.; Petrone, N.; Lee, C.-H.; Choi, M. S.; Lee, D.-Y.; Lee, C.; Yoo, W. J.; Watanabe, K.; *et al.* Flexible and Transparent MoS<sub>2</sub> Field-Effect Transistors on Hexagonal Boron Nitride-Graphene Heterostructures. *ACS Nano* **2013**, *7*, 7931–7936.

(14) Van der Zande, A. M.; Huang, P. Y.; Chenet, D. A.; Berkelbach, T. C.; You, Y.; Lee, G.-H.; Heinz, T. F.; Reichman, D. R.; Muller, D. A.; Hone, J. C. Grains and Grain Boundaries in Highly Crystalline Monolayer Molybdenum Disulphide. *Nat. Mater.* **2013**, *12*, 554–561.

(15) Najmaei, S.; Liu, Z.; Zhou, W.; Zou, X.; Shi, G.; Lei, S.; Yakobson, B. I.; Idrobo, J.-C.; Ajayan, P. M.; Lou, J. Vapour Phase Growth and Grain Boundary Structure of Molybdenum Disulphide Atomic Layers. *Nat. Mater.* **2013**, *12*, 754–759.

(16) Novoselov, K. S.; Jiang, D.; Schedin, F.; Booth, T. J.; Khotkevich, V. V; Morozov, S. V; Geim, A. K. Two-Dimensional Atomic Crystals. *Proc. Natl. Acad. Sci. U. S. A.* **2005**, *102*, 10451–10453.

(17) Alem, N.; Yazyev, O. V; Kisielowski, C.; Denes, P.; Dahmen, U.; Hartel, P.; Haider, M.; Bischoff, M.; Jiang, B.; Louie, S. G.; *et al.* Probing the Out-of-Plane Distortion of Single Point Defects in Atomically Thin Hexagonal Boron Nitride at the Picometer Scale. *Phys. Rev. Lett.* **2011**, *106*.

(18) Gibb, A. L.; Alem, N.; Chen, J.-H.; Erickson, K. J.; Ciston, J.; Gautam, A.; Linck, M.; Zettl, A. Atomic Resolution Imaging of Grain Boundary Defects in Monolayer Chemical Vapor Deposition-Grown Hexagonal Boron Nitride. *J. Am. Chem. Soc.* **2013**, *135*, 6758–6761.

(19) Chen, L.; Liu, B.; Abbas, A. N.; Ma, Y.; Fang, X.; Liu, Y.; Zhou, C. Screw-Dislocation-Driven Growth of Two-Dimensional Few-Layer and Pyramid-like WSe<sub>2</sub> by Sulfur-Assisted Chemical Vapor Deposition. *ACS Nano* *0*, null.

(20) Zhang, L.; Liu, K.; Wong, A. B.; Kim, J.; Hong, X.; Liu, C.; Cao, T.; Louie, S. G.; Wang, F.; Yang, P. Three-Dimensional Spirals of Atomic Layered MoS<sub>2</sub>. *Nano Lett.* **2014**.

(21) Zhu, J.; Peng, H.; Marshall, A. F.; Barnett, D. M.; Nix, W. D.; Cui, Y. Formation of Chiral Branched Nanowires by the Eshelby Twist. *Nat. Nanotechnol.* **2008**, *3*, 477–481.

(22) Morin, S. A.; Jin, S. Screw Dislocation-Driven Epitaxial Solution Growth of ZnO Nanowires Seeded by Dislocations in GaN Substrates. *Nano Lett.* **2010**, *10*, 3459–3463.

(23) Meng, F.; Morin, S. A.; Forticaux, A.; Jin, S. Screw Dislocation Driven Growth of Nanomaterials. *Acc. Chem. Res.* **2013**, *46*, 1616–1626.

(24) Zhuang, A.; Li, J.-J.; Wang, Y.-C.; Wen, X.; Lin, Y.; Xiang, B.; Wang, X.; Zeng, J. Screw-Dislocation-Driven Bidirectional Spiral Growth of Bi<sub>2</sub>Se<sub>3</sub> Nanoplates. *Angew. Chemie* **2014**, *126*, 6543–6547.

(25) Mak, K. F.; Lee, C.; Hone, J.; Shan, J.; Heinz, T. F. Atomically Thin MoS<sub>2</sub>: A New Direct-Gap Semiconductor. *Phys. Rev. Lett.* **2010**, *105*.

(26) Splendiani, A.; Sun, L.; Zhang, Y. B.; Li, T. S.; Kim, J.; Chim, C. Y.; Galli, G.; Wang, F. Emerging Photoluminescence in Monolayer MoS<sub>2</sub>. *Nano Lett.* **2010**, *10*, 1271–1275.

(27) Lu, N.; Guo, H.; Li, L.; Dai, J.; Wang, L.; Mei, W.-N.; Wu, X.; Zeng, X. C. MoS<sub>2</sub>/MX<sub>2</sub> Heterobilayers: Bandgap Engineering via Tensile Strain or External Electrical Field. *Nanoscale* **2014**, *6*, 2879–2886.

(28) Kim, K.; Coh, S.; Tan, L. Z.; Regan, W.; Yuk, J. M.; Chatterjee, E.; Crommie, M. F.; Cohen, M. L.; Louie, S. G.; Zettl, A. Raman Spectroscopy Study of Rotated Double-Layer Graphene: Misorientation-Angle Dependence of Electronic Structure. *Phys. Rev. Lett.* **2012**, *108*, 246103.